EFFECT OF ELECTRON TRANSPORT LAYERS, INTERFACE DEFECT DENSITY AND WORKING TEMPERATURE ON PEROVSKITE SOLAR CELLS USING SCAPS 1-D SOFTWARE

Abubakar S. Yusuf[a,b]*, A.M. Ramalan[c], A.A. Abubakar[a], I.K. Mohammed[a]

a Department of Physics, Federal University of Technology, P.M.B. 65, Minna, Nigeria
b Department of Physics and Astronomy, Auckland University of Technology, New Zealand
c Department of Physics, University of Abuja, P.M.B. 117, Abuja, Nigeria
Corresponding Author e-mail: ayusuf@futminna.edu.ng, abubakar.yusuf@autuni.ac.nz
Received November 29, 2023; revised December 17, 2023; accepted December 30, 2023

Perovskite solar cells have garnered significant attention from solar cell researchers due to their potential for achieving high efficiency, primarily attributed to their exceptional Electron Transport layer (ETL). One of the key elements of perovskite solar cells for transporting electrons to generate current is the ETL material. Moreover, there is a promising avenue for enhancing stability and reducing fabrication costs by substituting the transport layer. In this study, TiO_2 and SnO_2 were used as ETL materials in the architecture of perovskite solar cells for a comparative analysis between two devices featuring distinct structures: $TiO_2/CH_3NH_3PbI_3$/Spiro-OMeTAD and $SnO_2/CH_3NH_3PbI_3$/Spiro-OMeTAD. To evaluate the performance of each electron transport layer (ETL), the SCAPS 1D tool was employed. The investigation involved varying the thickness of the electron transport layers, interface defect density and working temperature, allowing for a comprehensive assessment of key parameters such as voltage at open circuit (Voc), short circuit current density (Jsc), fill factor (FF), and overall efficiency (PCE%). Remarkably, when employing SnO_2 as the ETL, the achieved efficiency stands at 10.10 %. In contrast, utilizing TiO_2 as the ETL yields a slightly higher efficiency of 12.84%. These findings underline the nuanced influence of transport layer materials on the overall performance of perovskite solar cells.
Keywords: *Perovskite; Solar cell; SCAP-1D*
PACS: 02.60.Cb, 61.72.-y, 42.79.Ek, 84.60.Jt

INTRODUCTION

Global worries about the depletion of fossil fuels have led to an increasing demand for renewable energy sources considering recent technological advancements. Permanent resources may be provided by renewable energy; all that is needed for researchers to take use of these natural resources is to broaden their study scope. Solar energy is among the most promising renewable energy sources [1]. As a result, creating a new solar cell technology with higher power conversion efficiency (PCE) and lower processing costs will take a great deal of work. These days, organic and inorganic halide perovskite solar cells are simple to fabricate in a variety of locations, meet the aforementioned properties, and offer intrinsic benefits such as a high absorption coefficient, long carrier-diffusion length, and high carrier mobility [2]. They are thus very desirable for the next solar cell technologies. However, Kojima et al. from Tsutomu Miyasaka's Tokyo-based company built the first perovskite solar cell with a PCE of 2.2% in 2006 [3] and after a few years, they enhanced it to 3.8% [4]. Therefore, in less than one decade, perovskite-based solar cells jumped to a PCE of 25.2% in 2019 [5]. Enhancement of the device structure and perovskite material is the key to improving the performance of perovskite-based solar cells. The use of perovskite solar cells using methylammonium lead tri-iodide-based perovskite material is the subject of many investigations ($MAPbI_3$). This later is composed of ABX_3 structure, where A represents methylammonium (MA, CH_3NH_3), B is lead (Pb) and X represents a halide material anion, iodide (I). Despite the high performance provided by lead halide perovskite material, the factor of instability and toxicity may hamper its commercial production [6-8]. The better way to improve these factors, More recently, several mixed halide perovskite materials have been widely implemented as absorber layers in PSCs to further enhance the efficiency and stability [9], Ito et al. examined PSC with mixed Sn–Ge perovskite absorber layer ($FA_{0.75}MA_{0.25}Sn_{0.95}Ge_{0.05}I_3$) and reported PCE of 4.48% with improved stability in air due to the added Ge [10]. Afterwards, Ng et al. fabricated another mixed Sn–Ge perovskite cell and achieved PCE of 7.9%, short-circuit current density (J_{sc}) of 25.5 mA/cm^2, open-circuit voltage (V_{oc}) of 0.45 V and fill factor (FF) of 0.69 [11]. This far lower PCE of Sn–Ge-based PSCs in comparison with that of Pb-based PSCs is mainly attributed to their low open-circuit voltage which is due to the undesirable oxidation of Sn and consequently increased defect density [12]. In 2020, Minamoto et al. theoretically analysed mixed Sn–Ge perovskite solar cell with an inverted p-i-n planar structure and revealed that V_{oc} is strongly affected by built-in potential (V_{bi}) across the perovskite absorber layer, where V_{bi} is dominantly determined by the conduction band minimum (CBM) of the electron transport layer (ETL) and/or work function of back contact [9]. They showed that by optimizing the conduction band offset of perovskite and ETL as well as choosing suitable back contact, an improved V_{oc} of 0.93 V (PCE of 19.4%) can be achieved [9, 13]. According to the properties of Pb-, Sn-, Ge- and SnGe- based perovskites, we think that an appropriate combination of these layers as absorber layers in PSCs may lead to better performance in a wider range of solar spectrum. In this line of thought, Farhadi et al. [13] very recently have simulated and investigated a perovskite solar cell with a double absorber layer ($MASnI_3/MAPbI_3$) and achieved a high PCE of 30.88%.

In this study, using SCAPS-1D simulation tool [14], we propose and simulate a novel PSC structure with double ETLs layers consisting of TiO_2 and SnO_2, TiO_2/SnO_2, and $TiO_2/SnO_2/MAPbI_3$ to take advantage of different ETLs important properties. Furthermore, we compare the output performance of the proposed cell with single and double ETL layers PSCs to show the efficiency improvement in double ETL layers PSC. Moreover, we concentrate on the effect of carrier transport materials, thickness of ETLs layers, interface defect density and working temperature on the efficiency of the proposed single and double ETL layers PSC. The improved performance of the proposed double ETL layers PSC can pave the path for further studies to fabricate experimentally and make benefit out of using double ETL layers layer in perovskite solar cells. Figure 1 and 2 display the perovskite solar cell layers using SCAPS-1D and SCAPS-1D define panel with each layers name.
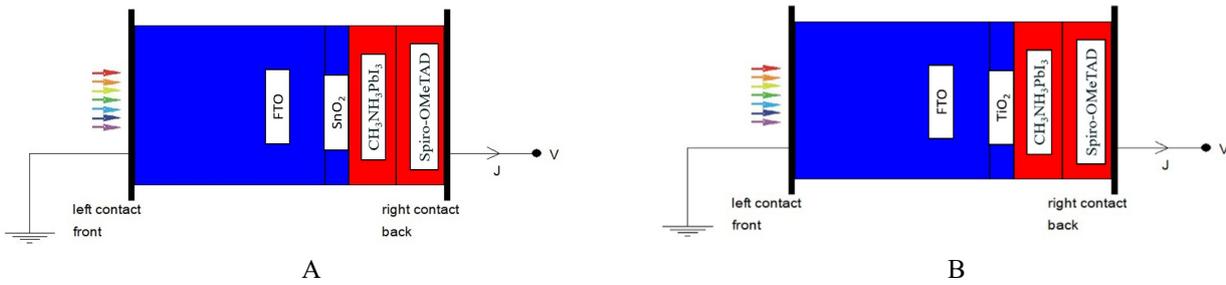

A   B

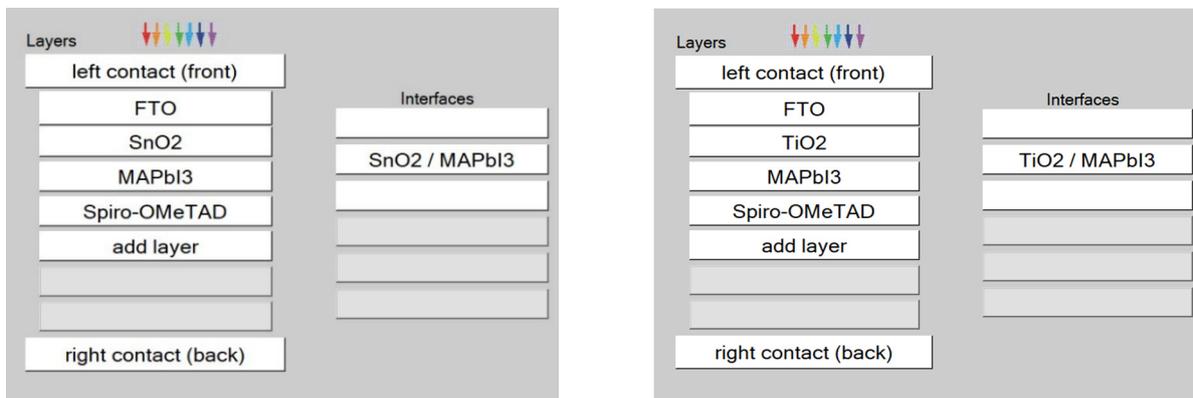**Figure 1.** Perovskite solar cell layer with SCAPS-1D

Figure 2. SCAPS-1D define panel with layers name

2. SCAPS-1D SIMULATION

A one-dimensional solar cell simulation tool will be used to replicate PSC and has been used to research several solar cell types, including CZTS, CIGS, and others [15, 16]. In contrast to other software, SCAPS features a very user-friendly operation window and a variety of grading, fault and recombination model options [17]. It acts like a real-life counterpart once all parameters have been defined [18]. Up to seven (7) semiconductor layers can be used to identify the primary characteristics of SCAPS, including the materials and defective attributes. By resolving the semiconductor fundamental equations, this software can simulate and help with the analysis of the J-V characteristics curve, the ac characteristics (C-V and C-f), the device's spectral response (QE), the open circuit voltage, the fill factor (FF), the short-circuit current (Jsc), and the power conversion efficiency (PCE) (Voc),the energy bands of the materials used in solar cells, and the concentration of various materials [19]. Figure 3 below shows the working procedure of a SCAPS-1D.
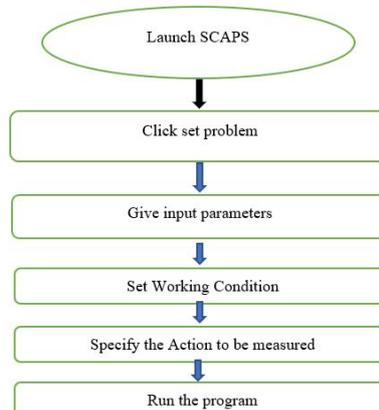

Figure 3. SCAPS working procedure

Numerical simulation was carried out using a software called The University of Gent created the Solar Cell Capacitance Simulator (SCAPS) [14] it was used to determine the influence of electron transport and perovskite active layers on solar cells parameters (Jsc, Voc, FF, and efficiency), various simulations were conducted to investigate the effects of ETLs with thicknesses ranging from 30 to 100 nm, the interface defect density (ETL/Perovskite absorber) varying from 10^{14} to 10^{19}, and the effect of temperature varying from 300 to 350K. The data used in the simulation and material parameters in SCAPS were implemented from theories and works of literature [20-25].

2.1. Numerical Simulation

The SCAPS-1D programme (solar cell capacitance simulator one dimension) was used to simulate solar cells by numerically resolving the one-dimensional Poisson and continuity equations that control semiconductor material under steady-state conditions [14]. The relationship between a p-n junction's electric field (E) and space charge density (ρ) is shown by the Poisson equation, which is represented by:

$$\frac{\partial^2 \varphi}{\partial^2 x} = \frac{\partial E}{\partial x} = -\frac{\rho}{\varepsilon_s} = -\frac{q}{\varepsilon_s}\left[p - n + N_D^+(x) - N_A^-(x) \pm N_t(x)\right] \tag{1}$$

Where N+, N, and Nt are the densities of ionized donors and acceptors, respectively, and where is the electrostatic potential, q is the elementary charge, s is the medium's static relative permittivity [26]. The following equations represent the electron and hole continuity in steady state:

$$\frac{\partial jn}{\partial x} + G - R_n(n,p) = 0 \tag{2}$$

$$-\frac{\partial jp}{\partial x} + G - R_p(n,p) = 0 \tag{3}$$

where Rn, Rp are the net rates of electron and hole recombination, G is the rate at which electron-hole pairs are created, and jn, jp are the current densities of electrons and holes. These equations provide the electron and hole current densities:

$$jn = qu\mu_n E + qD_n\frac{\partial n}{\partial x} \tag{4}$$

$$jp = qp\mu_n E + qD_p\frac{\partial p}{\partial x} \tag{5}$$

where q is the fundamental charge, n, p are the electron and hole mobilities, and Dn, Dp are the electron and hole diffusion coefficients. The SCAPS-1D program can simulate solar cells with up to seven layers and extract the fundamental properties of the cells, including their band diagram, generation and recombination rates, external quantum efficiency, cell current densities, J-V characteristic include power conversion efficiency, fill factor, open-circuit voltage, and short-circuit current.

To have a successful replication of the simulation carried out by [27], The simulation's parameters are taken from literature, experimental research, and theoretical study. The details for each layer are summarized in Table 1 [28-33].

**Table 1.** perovskite solar cell input parameters [27].

Parameters	ITO [30, 31]	TiO$_2$ [29, 32]	SnO$_2$ [33]	MAPbI$_3$ (CH$_3$NH$_3$PbI$_3$) [34]	Spiro-OmeTAD [29]
Thickness (nm)	300	30	30	100	100
Band gap (eV)	3.6	3.26	3.5	1.51	2.9
Electron affinity (eV)	4.2	4.2	4.0	4.0	2.2
Dielectric permittivity	10	10	9.0	6.6	3
CB effective density of states (cm^{-3})	2.10^{18}	$2.2.10^{18}$	$2.2.10^{17}$	$1.2.10^{19}$	$2.2.10^{18}$
VB effective density of states (cm^{-3})	$1.8.10^{19}$	$1.8.10^{18}$	$2.2.10^{17}$	$2.9.10^{18}$	$1.8.10^{18}$
Thermal velocity of electrons (cm/s)	10^7	10^7	10^7	10^7	10^7
Thermal velocity of holes (cm/s)	10^7	10^7	10^7	10^7	10^7
Electron mobility (cm^2/Vs)	50	20	20	2.7	10^{-4}
Hole mobility (cm^2/Vs)	75	10	10	1.8	10^{-4}
Shallow donor density N_D (cm^{-3})	10^{19}	10^{17}	10^{15}	0	0
Shallow acceptor density N_A (cm^{-3})	0	0	0	$1.3.10^{16}$	10^{18}
Defect density N_t (cm^{-3})	10^{15}	10^{15}	10^{18}	4.10^{13}	10^{15}

3. RESULT AND DISCUSSION OF THE SIMULATION
3.1. Effect of the ETL (TiO$_2$) Thickness

Figure 4a show the *J–V* performance of the device with varying TiO$_2$ thickness from 30 to 100 nm under illumination and in the dark. **Figure 4b** displays the QE for different TiO$_2$ thicknesses versus wavelength. Our study's findings demonstrate that when TiO$_2$ thickness increases, all photovoltaic parameters rise as well. This is explained by the TiO$_2$ layer's fractional absorption of incoming light and its greater transmittance, which prevents solar irradiance from reaching the perovskite skeleton [35]. Ranging the thickness from 30 to 100 nm causes the QE versus wavelength curve

to have a spectrum overlap, which is explained by a constant optical absorption efficiency within the chosen thickness values. The ideal thickness of TiO_2 is 100 nm, demonstrating a PCE of 12.89%, FF of 84.29%, J_{sc} of 12.13 mA/ cm², and V_{oc} of 1.26 V.
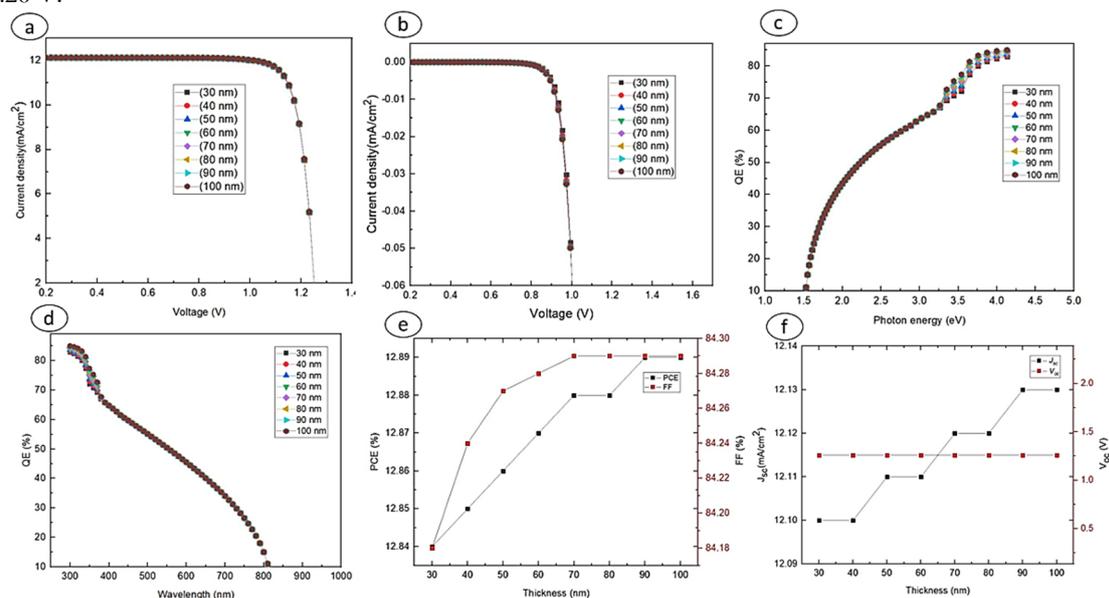
Figure 4. a - $J–V$ curve with varied ETM thickness under illumination; **b** - $J–V$ plot with varied ETM thickness in the dark; **c** - QE curve with respect to photon energy; **d** - QE curve with respect to wavelength; **e** - PCE and FF with respect to thickness, and **f** - J_{sc} and V_{oc} with respect to varied ETM thickness

### 3.2. Effect of the ETL (SnO_2) Thickness

Figure 5a show the $J–V$ performance of the device with varying SnO_2 thickness from 30 to 100 nm under illumination and in the dark. **Figure 5b** shows the QE against wavelength for varying SnO_2 thicknesses. The findings of our study demonstrate that as SnO_2 thickness increases, all photovoltaic parameters drop. This is explained by the SnO_2 layer's fractional absorption of incoming light and its reduced transmittance, which inhibits solar irradiance on the perovskite skeleton [35]. Ranging the thickness from 30 to 100 nm leads to a spectrum overlap in the QE versus wavelength graph. This is explained by the optical absorption efficiency being constant throughout the chosen thickness ranges. The optimum SnO_2 thickness is 30 nm, demonstrating a PCE of 10.10%, FF of 69.40%, J_{sc} of 12.07 mA/ cm², and V_{oc} of 1.20 V.
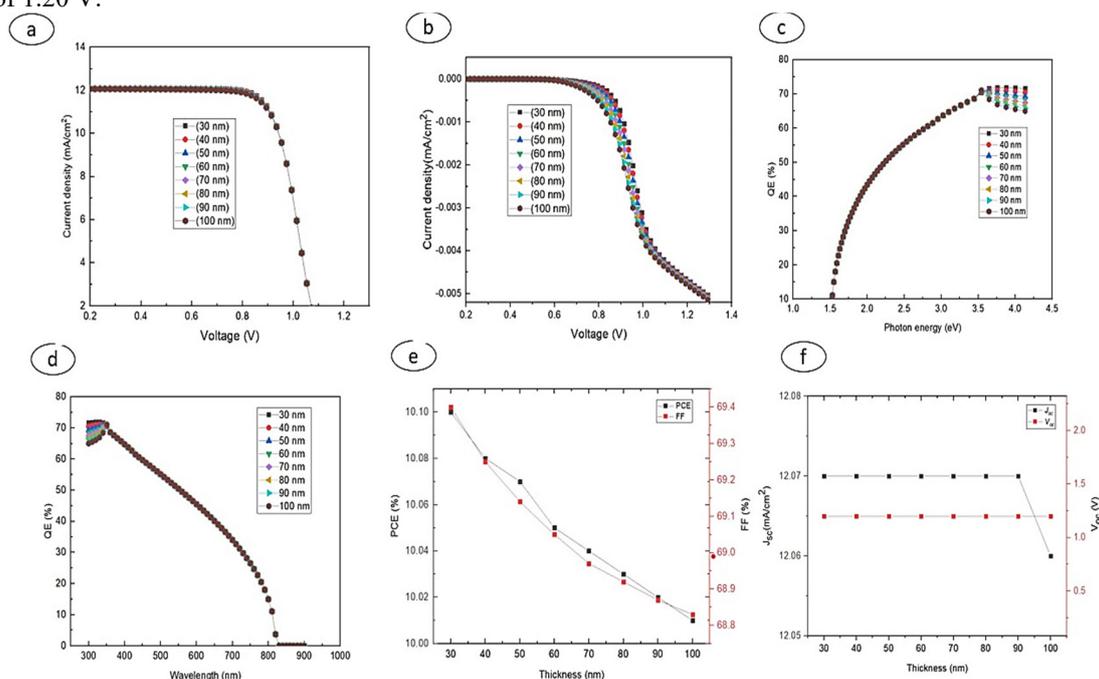
Figure. 5. a - $J–V$ curve with varied ETM thickness under illumination; **b** - $J–V$ plot with varied ETM thickness in the dark; **c** - QE curve with respect to photon energy; **d** - QE curve with respect to wavelength; **e** - PCE and FF with respect to thickness, and **f** - J_{sc} and V_{oc} with respect to varied ETM thickness

3.3 Effect of the ETL (TiO₂/SnO₂) Thickness

First, we may clarify the stability in FF; FF indicates the caliber of the solar cell and is connected to the characteristics of the active layer. Because V_{oc} and E_g have a relationship, the perovskite layer band gap remains unchanged, which accounts for V_{oc} stability. The increase in light absorption in the TiO_2/SnO_2 layer with increasing layer thickness is the second factor contributing to the decline in J_{sc}. More proof can be drawn from examining the quantum efficiency curve, which indicates that this has an impact on the number of photons transmitted to the active layer (in this case, Perovskite), which then leads to a reduction in the photo-generated carriers in these layers. The quantum efficiency at short wavelengths increases with increasing TiO_2/SnO_2 thickness (300-380 nm). The short wavelengths are known to be absorbed close to the solar cell's surface and away from the effective region. As a result, fewer carriers are produced to produce the desired effects, which reduces the short-circuit current. where the relationship between the quantum efficiency and the short circuit current density is direct. Solar cell's power conversion efficiency (PCE) also drops as the J_{sc} falls [36]. The optimum TiO_2/SnO_2 thickness is 30 nm, demonstrating a PCE of 12.68%, FF of 83.48%, J_{sc} of 12.09 mA/cm², and V_{oc} of 1.25 V.
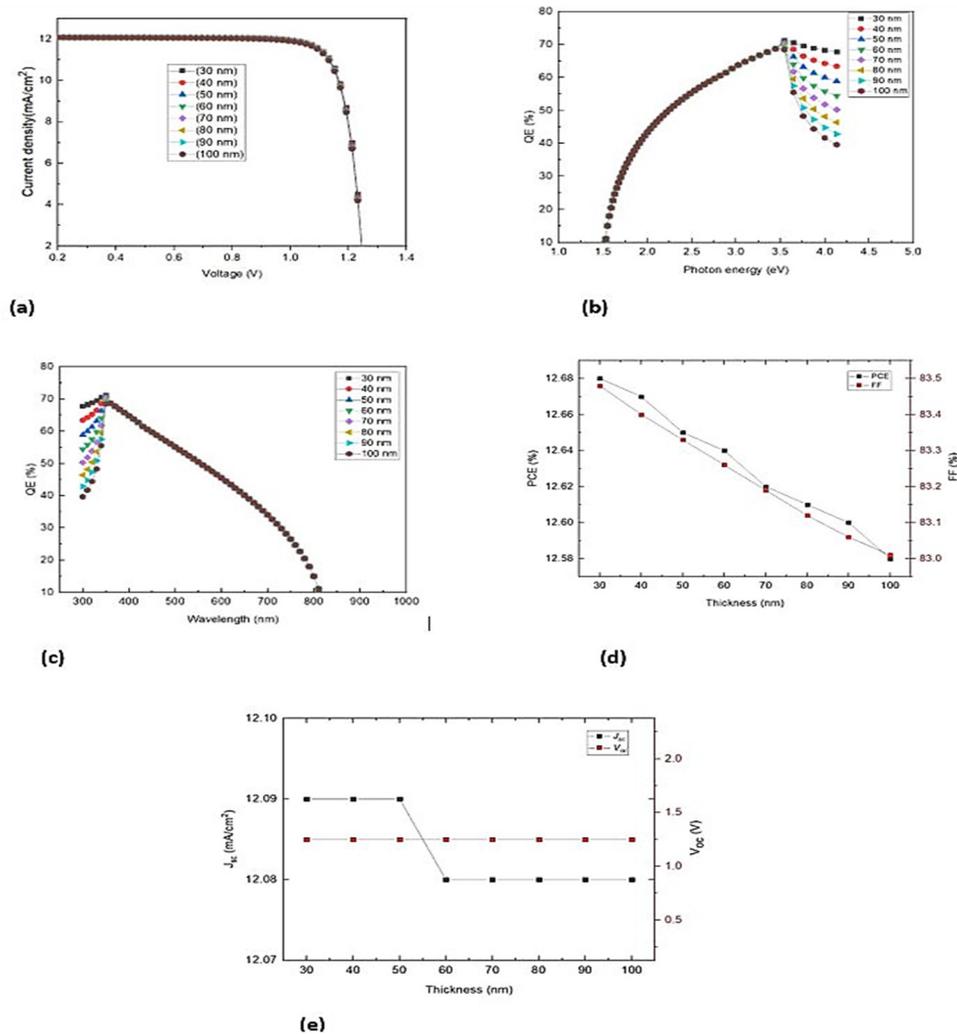
Figure 6. **a** *J–V* curve with varied ETM thickness under illumination. **b** QE curve concerning photon energy. **c** QE curve concerning wavelength. **d** PCE and FF concerning thickness and **e** J_{sc} and V_{oc} concerning varied ETM thickness

### 3.4 Effect of Interface defect density TiO₂/MAPbI₃

Due to the discontinuity in structure of solar cells, there is a high likelihood of introducing localised defect states between two-layer interfaces. Minority carrier recombination velocities are the best way to quantify the impact of defect interface density [37]. To investigate how the interface flaw affects the $TiO_2/MAPbI_3$ interface of PSCs, the N_t was varied from 10^{14} to 10^{19} cm^{-2} while keeping other parameters unchanged. **Figure 7a** shows the *J–V* curve with varied interface defects, while **Figure 7b** shows the PCE and FF concerning the interface defect, and **Figure 7c** depicts the J_{sc} and V_{oc} in relation to the defect density at the contact. Based on the findings, the photovoltaic parameters (PCE, FF, J_{sc}, and V_{oc}) decreased with increasing the defect density from 10^{14} to 10^{19} cm^{-2}. Consequently, while creating PSCs with a high PCE, the interface modification and film morphology to control Nt must be carefully managed. The optimum $TiO_2/MAPbI_3$ interface defect density is 10^{14} cm^{-2}, demonstrating a PCE of 10.19 %, FF of 82.19 %, J_{sc} of 12.10 mA/ cm², and V_{oc} of 1.02 V.
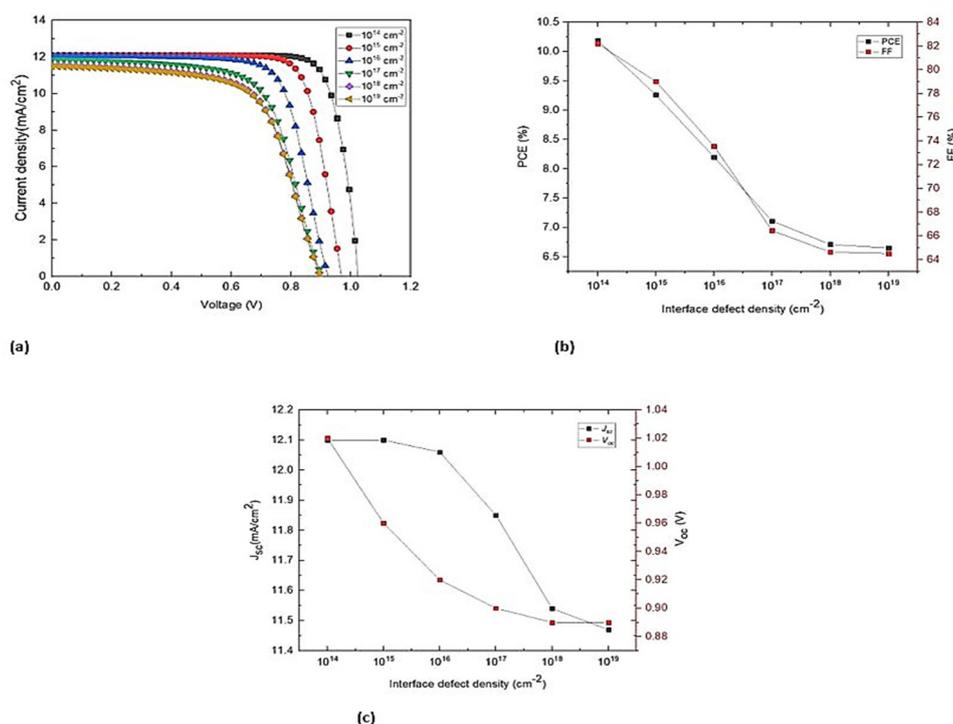
Figure 7. a J–V curve with varied interface defect density. **b** The correlations of PCE and FF with interface defect and **c** J_{sc} and V_{oc} with interface defect density

3.5. Effect of Interface defect density on SnO₂/MAPbI₃

It is common for localized defect states to be introduced between two-layer interfaces because of the structural discontinuity in solar cells. Minority carrier recombination velocities provide the most accurate way to articulate the impact of defect interface density [37]. To investigate the impact the interface flaw has on the SnO_2/MAPbI₃ interface of PSCs, the N_t was varied from 10^{14} to 10^{19} cm^{-2} while keeping other parameters unchanged.
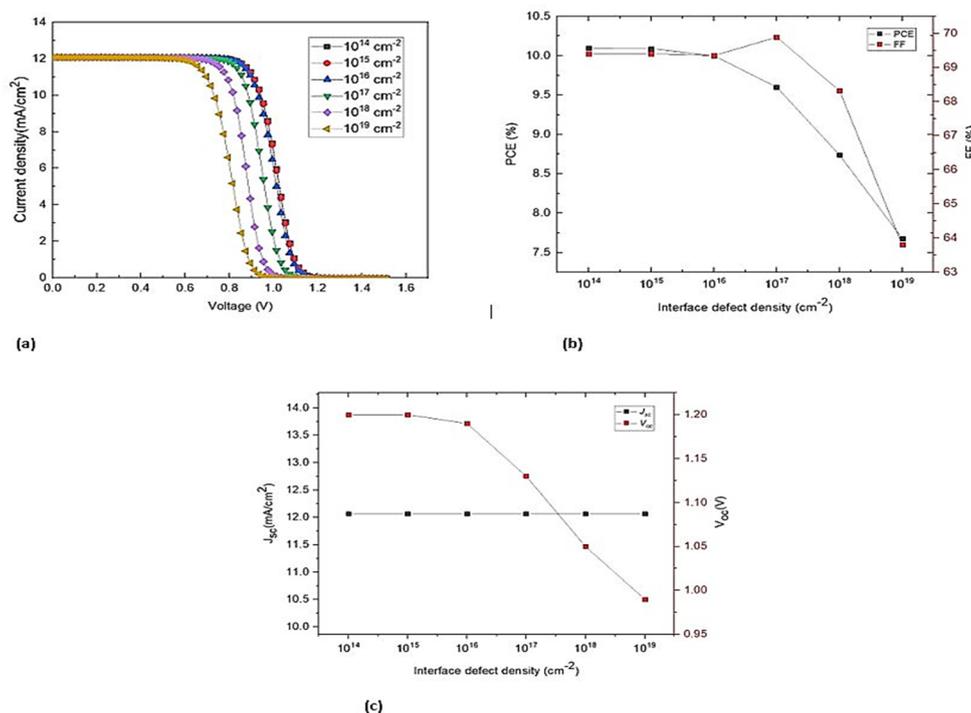
Figure 8. a J–V curve with varied interface defect density. **b** The correlations of PCE and FF with interface defect and **c** J_{sc} and V_{oc} with interface defect density.

Figure 8a shows the J–V curve with varied interface defects, while **Figure 8b** shows the PCE and FF concerning the interface defect, and **Figure 8c** depicts the J_{sc} and V_{oc} concerning the interface defect density. From the results

obtained, the photovoltaic parameters (PCE, FF, and V_{oc}) decreased with increasing the defect density from 10^{14} to 10^{19} cm^{-2} while J_{sc} remained unaltered. Consequently, while creating PSCs with a high PCE, the interface modification and film morphology to control Nt must be carefully managed. The optimum SnO$_2$/MAPbI$_3$ interface defect density is 10^{14} cm^{-2} demonstrating a PCE of 10.10 %, FF of 69.40 %, J_{sc} of 12.07 mA/cm^2, and V_{oc} of 1.20 V.

3.6 Effect of Temperature on ETL (TiO₂)

An essential aspect in determining a solar cell device's output is its temperature. We used simulation to expose our gadget to temperatures between 300 and 350 K to examine its impact on its performance. When light is absorbed, PSC's temperature may rise and commonly rises beyond 300 K. [38]. **Figure 9. a–c** displays the temperature-dependent current density, PCE and FF, Jsc and Voc.

In the current study, PCE, Jsc, Voc, and FF all drop as temperature rises. This might be the result of the electron reaching an unstable state at a higher temperature after absorbing enough photons, which increases the rate of recombination and lowers the PCE, Jsc, Voc, and FF [39]. The optimum TiO₂ temperature is 300 K, demonstrating a PCE of 10.10 %, FF of 69.40 %, J_{sc} of 12.07 mA/ cm^2, and V_{oc} of 1.20 V.

(a)

(b)

(c)
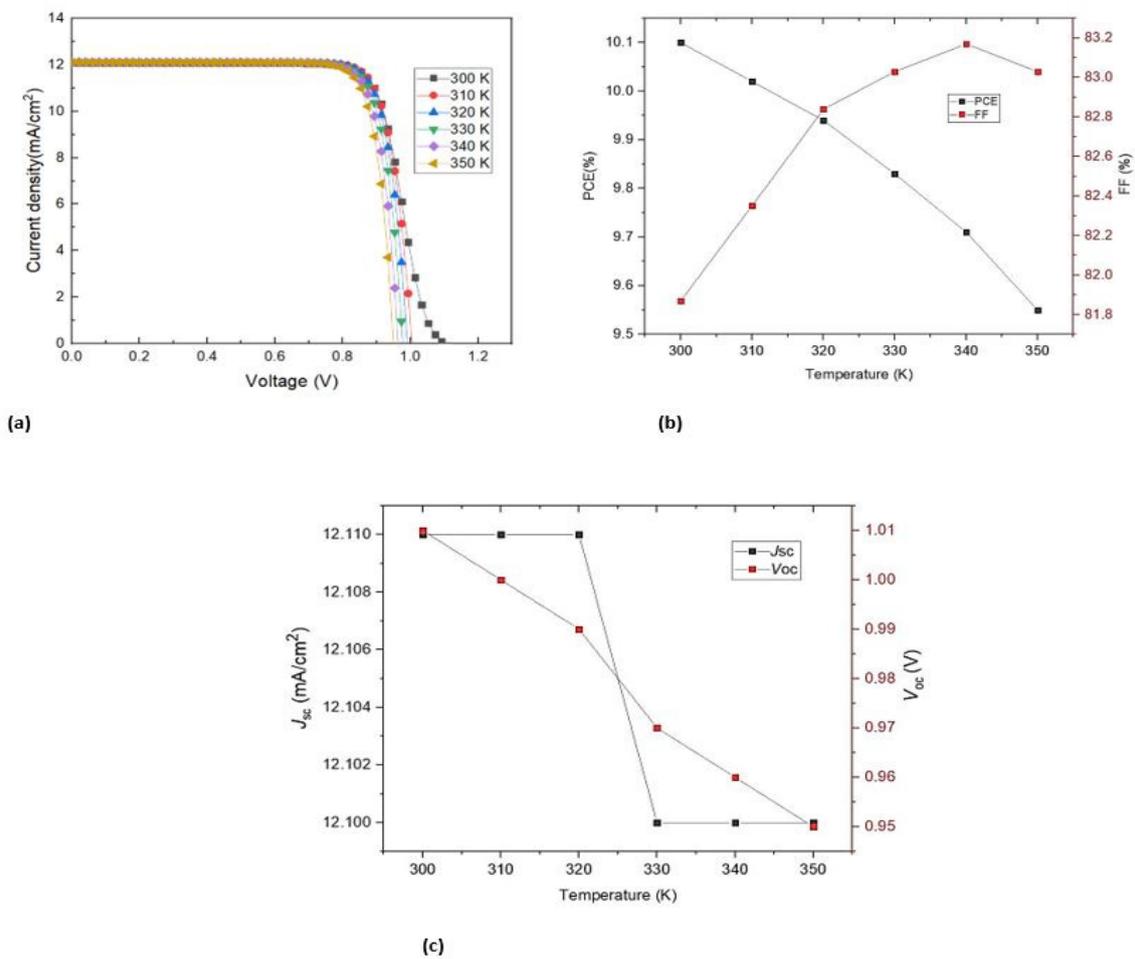
Figure 9. a *J–V* curve as a function of temperature. **b** Correlation of PCE and FF with temperature. **c** Correlation of J_{sc} and V_{oc} with temperature.

3.7 Effect of Temperature on ETL (SnO₂)

For solar cell devices output, temperature is a crucial determining element. Utilizing simulation, we subjected the device to temperatures between 300 and 350 K to examine its impact on the performance of our technology. When light is absorbed, PSC's temperature may rise and commonly rises beyond 300 K [38]. **Figure 10. a–c** shows the current density, PCE and FF, and Jsc and Voc in relation to temperature. The current study shows that a rise in temperature causes a fall in PCE, Jsc, Voc, and FF. This might be as a result of the electron reaching an unstable state and absorbing enough photons at a higher temperature, which increases the rate of recombination and lowers the PCE., Jsc, and Voc [39]. The optimum SnO₂ temperature is 300 K, demonstrating a PCE of 8.52 %, FF of 67.22 %, J_{sc} of 12.07 mA/ cm^2, and V_{oc} of 1.04 V.
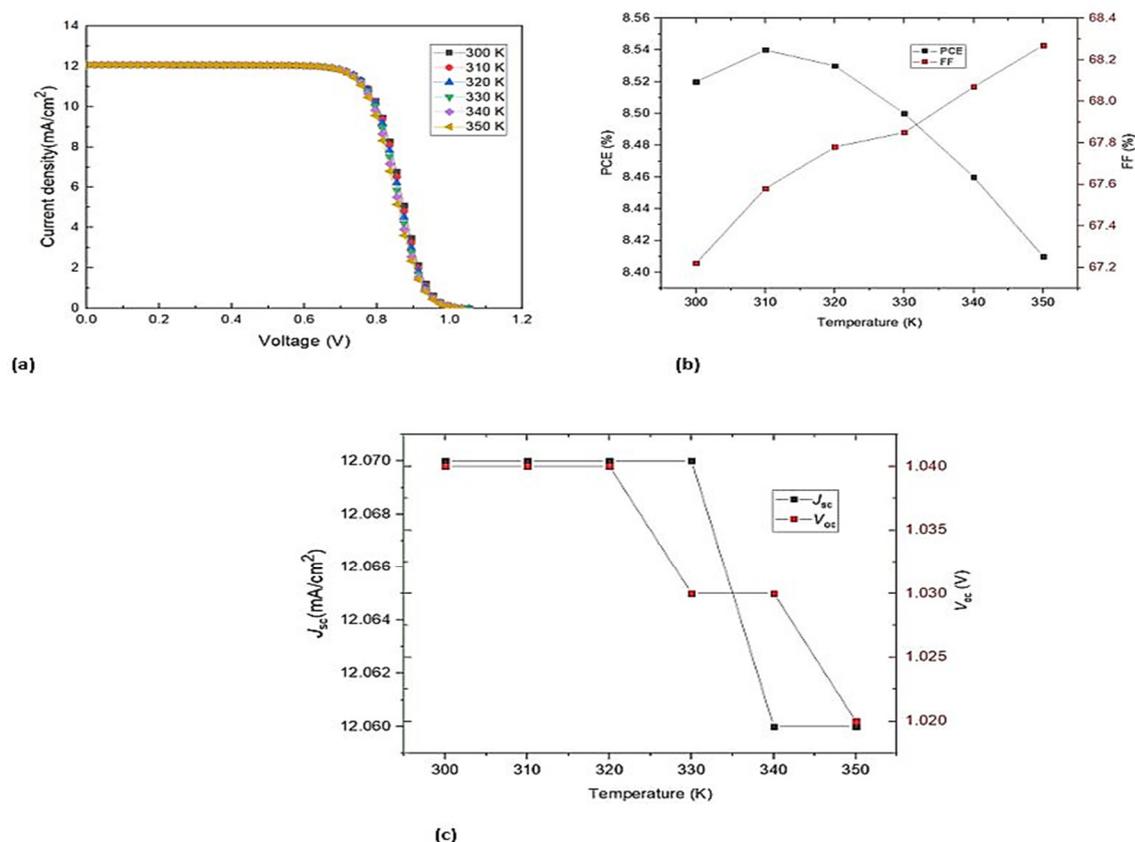
Figure 10. a - $J–V$ curve as a function of temperature; **b** - Correlation of PCE and FF with temperature;. **c** - Correlation of J_{sc} and V_{oc} with temperature.

4. SUMMARY OF THE SIMULATION RESULTS

In this work, the perovskite solar cell structure $TiO_2/CH_3NH_3PbI_3/Spiro-OMeTAD$ and $SnO_2/CH_3NH_3PbI_3/Spiro-OMeTAD$ is numerically modeled by carefully varying the effect of ETLs thickness, interface defect density and working temperature on charge carriers of the electron transport and perovskite active layers on the solar cells, we can conclude from the results obtained above that the thickness and temperature did not significantly enhance the device power conversion efficiency. But instead, the interface defect density had a significant enhancement on the device power conversion efficiency for both $TiO_2/$ MAPbI$_3$ and SnO_2/MAPbI$_3$ which was found out to be at $10^{14} cm^{-2}$ with optimum values of PCE of 10.19 %, FF of 82.19 %, J_{sc} of 12.10 mA/ cm^2, and V_{oc} of 1.02 V and PCE of 10.10 %, FF of 69.40 %, J_{sc} of 12.07 mA/ cm^2, and V_{oc} of 1.20 V respectively. It could be concluded that the electron transport and perovskite active materials can transmit and absorb the light intensity of the photons and exhibit that by optimizing the interface defect density parameter, the device power conversion efficiency could be increased to a higher efficiency.

Declaration of Competing Interest
The authors declare that they have no known competing financial interests or personal relationships that could have influenced the work reported in this study.
Data Availability
Data will be made available on request.

Abubakar Sadiq Yusuf, https://orcid.org/0000-0001-8181-9728

REFERENCES
[1]   P. Kumar, S. Kumar, A.A. Adelodun, and K.-H. Kim, "Solar energy: Potential and future prospects," Renewable and Sustainable Energy Reviews, **82**, 894-900 (2018). https://doi.org/10.1016/j.rser.2017.09.094
[2]   I. Kemerchou, F. Rogti, B. Benhaoua, A. Hima, and A. Khechekhouche, "Characterization of organic/inorganic perovskite material CH3NH3PbI3 prepared by spray pyrolysis with moving nozzle method," Recueil De Mécanique, **4**(1), 342–348 (2019). https://doi.org/10.5281/zenodo.3447388
[3]   A. Kojima, K. Teshima, T. Miyasaka, and Y. Shirai, "Novel photoelectrochemical cell with mesoscopic electrodes sensitized by lead-halide compounds," ECS Meeting Abstracts, **MA2006-02**, 397 (2006). https://doi.org/10.1149/MA2006-02/7/397

[4]   A. Kojima, K. Teshima, Y. Shirai, and T. Miyasaka, "Organometal halide perovskites as visible-light sensitizers for photovoltaic cells," Journal of the american chemical society, **131**(17), 6050-6051 (2009). https://doi.org/10.1021/ja809598r

[5]   NREL, *National renewable energy laboratory: best research-cell efficiency chart,* (2021). https://www.nrel.gov/pv/cell-efficiency.html

[6]   M.K. Assadi, S. Bakhoda, R. Saidur, and H. Hanaei, "Recent progress in perovskite solar cells," Renewable and Sustainable Energy Reviews, **81**, 2812-2822 (2018). https://doi.org/10.1016/j.rser.2017.06.088

[7]   P. Cheng, and X. Zhan, "Stability of organic solar cells: challenges and strategies," Chemical Society Reviews, **45**(9), 2544-2582 (2016). https://doi.org/10.1039/C5CS00593K

[8]   L.P. Lekesi, L.F. Koao, S.V. Motloung, T.E. Motaung, and T. Malevu, "Developments on Perovskite Solar Cells (PSCs): A Critical Review," Applied Sciences, **12**(2), 672 (2022). https://doi.org/10.3390/app12020672

[9]   T. Minemoto, Y. Kawano, T. Nishimura, Q. Shen, K. Yoshino, S. Iikubo, S. Hayase, and J. Chantana, "Theoretical analysis of band alignment at back junction in Sn–Ge perovskite solar cells with inverted p-i-n structure," Solar Energy Materials and Solar Cells, **206**, 110268 (2020). https://doi.org/10.1016/j.solmat.2019.110268

[10]   N. Ito, M.A. Kamarudin, D. Hirotani, Y. Zhang, Q. Shen, Y. Ogomi, S. Iikubo, et al., "Mixed Sn–Ge perovskite for enhanced perovskite solar cell performance in air," The journal of physical chemistry letters, **9**(7), 1682-1688 (2018). https://doi.org/10.1021/acs.jpclett.8b00275

[11]   M. Ng, and J.E. Halpert, "Single crystals of mixed Br/Cl and Sn-doped formamidinium lead halide perovskites via inverse temperature crystallization," RSC Adv, **10**(7), 3832-3836 (2020). https://doi.org/10.1039/D0RA00060D

[12]   N.-G. Park, "Organometal perovskite light absorbers toward a 20% efficiency low-cost solid-state mesoscopic solar cell," The Journal of Physical Chemistry Letters, **4**(15), 2423-2429 (2013). https://doi.org/10.1021/jz400892a

[13]   B. Farhadi, M. Ciprian, F. Zabihi, and A. Liu, "Influence of contact electrode and light power on the efficiency of tandem perovskite solar cell: Numerical simulation," Solar Energy, **226**, 161-172 (2021). https://doi.org/10.1016/j.solener.2021.08.043

[14]   M. Burgelman, P. Nollet, and S. Degrave, "Modelling polycrystalline semiconductor solar cells," Thin solid films, **361**, 527-532 (2000). https://doi.org/10.1016/S0040-6090(99)00825-1

[15]   Y.H. Khattak, Doct. Thesis, Modeling of high power conversion efficiency thin film solar cells, Universitat Politècnica de València, 2019. https://doi.org/10.4995/Thesis/10251/118802

[16]   M. Burgelman, K. Decock, A. Niemegeers, J. Verschraegen, and S. Degrave, *SCAPS manual,* (University of Gent Department of Electronics and Information Systems (ELIS) Campus Ardoyen, Technologiepark 914, Grote Steenweg Noord 9052 Gent-Zwijnaarde 'Belgium', 2016).

[17]   A. Husainat, W. Ali, P. Cofie, J. Attia, and J. Fuller, "Simulation and analysis of methylammonium lead iodide (CH3NH3PbI3) perovskite solar cell with Au contact using SCAPS 1D simulator," American Journal of Optics and Photonics, **7**(2), 33 (2019). https://doi.org/10.11648/j.ajop.20190702.12

[18]   B.M. Soucase, I.G. Pradas, and K.R. Adhikari, "Numerical simulations on perovskite photovoltaic devices," in: *Perovskite Materials - Synthesis, Characterisation, Properties, and Applications*, edited by L. Pan, and G. Zhu, **445**, (IntechOpen, 2016). https://doi.org/10.5772/61751

[19]   Hazeghi, F. and S.M.B. Ghorashi, "Simulation of perovskite solar cells by using CuSCN as an inorganic hole-transport material," Materials Research Express, **6**(9), 095527 (2019). https://doi.org/10.1088/2053-1591/ab2f1b

[20]   T. Pu, H. Shen, and Q. Tang, "Simulation of a charged Al2O3 film as an assisting passivation layer for a-Si passivated contact P-type silicon solar cells," Silicon, **14**(7), 3339-3348 (2022). https://doi.org/10.1007/s12633-021-01105-4

[21]   S.T. Jan, and M. Noman, "Influence of layer thickness, defect density, doping concentration, interface defects, work function, working temperature and reflecting coating on lead-free perovskite solar cell," Solar Energy, **237**, 29-43 (2022). https://doi.org/10.1016/j.solener.2022.03.069

[22]   R. Kotipalli, B. Vermang, J. Joel, R. Rajkumar, M. Edoff, and D. Flandre, "Investigating the electronic properties of Al2O3/Cu(In, Ga) Se2 interface," AIP Advances, **5**(10), 107101 (2015). https://doi.org/10.1063/1.4932512

[23]   K. Tan, P. Lin, G. Wang, Y. Liu, Z. Xu, and Y. Lin, "Controllable design of solid-state perovskite solar cells by SCAPS device simulation," Solid-State Electronics, **126**, 75-80 (2016). https://doi.org/10.1016/j.sse.2016.09.012

[24]   H. Abedini-Ahangarkola, S. Soleimani-Amiri, and S.G. Rudi, "Modeling and numerical simulation of high efficiency perovskite solar cell with three active layers," Solar Energy, **236**, 724-732 (2022). https://doi.org/10.1016/j.solener.2022.03.055

[25]   J. Lontchi, M. Zhukova, M. Kovacic, J. Krc, W.-C. Chen, M. Edoff, S. Bose, et al., "Optimization of Back Contact Grid Size in Al2O3-Rear-Passivated Ultrathin CIGS PV Cells by 2-D Simulations," IEEE Journal of Photovoltaics, **10**(6), 1908-1917 (2020). https://doi.org/10.1109/JPHOTOV.2020.3012631

[26]   T. Minemoto, and M. Murata, "Impact of work function of back contact of perovskite solar cells without hole transport material analyzed by device simulation," Current Applied Physics, **14**(11), 1428-1433 (2014). https://doi.org/10.1016/j.cap.2014.08.002

[27]   D. Stanić, V. Kojić, T. Čižmar, K. Juraić, L. Bagladi, J. Mangalam, T. Rath, and A. Gajović, "Simulating the performance of a formamidinium based mixed cation lead halide perovskite solar cell," Materials, **14**(21), 6341 (2021). https://doi.org/10.3390/ma14216341

[28]   S. Abdelaziz, A. Zekry, A. Shaker, and M. Abouelatta, "Investigating the performance of formamidinium tin-based perovskite solar cell by SCAPS device simulation," Optical Materials, **101**, 109738 (2020). https://doi.org/10.1016/j.optmat.2020.109738

[29]   S. Bansal, and P. Aryal, "Evaluation of new materials for electron and hole transport layers in perovskite-based solar cells through SCAPS-1D simulations," in: *2016 IEEE 43rd Photovoltaic Specialists Conference (PVSC),* (IEEE, 2016). pp.1-4. https://doi.org/10.1109/PVSC.2016.7749702

[30]   H.-J. Du, W.-C. Wang, and J.-Z. Zhu, "Device simulation of lead-free CH3NH3SnI3 perovskite solar cells with high efficiency," Chinese Physics B, **25**(10), 108802 (2016). https://doi.org/10.1088/1674-1056/25/10/108802

[31]   D. Liu, and T.L. Kelly, "Perovskite solar cells with a planar heterojunction structure prepared using room-temperature solution processing techniques," Nature photonics, **8**(2), 133-138 (2014). https://doi.org/10.1038/nphoton.2013.342

[32]   M.D. Stamate, "On the dielectric properties of dc magnetron TiO2 thin films," Applied Surface Science, **218**(1-4), 318-323 (2003). https://doi.org/10.1016/S0169-4332(03)00624-X

[33] S. Karthick, S. Velumani, and J. Bouclé, "Experimental and SCAPS simulated formamidinium perovskite solar cells: A comparison of device performance," Solar Energy, **205**, 349-357 (2020). https://doi.org/10.1016/j.solener.2020.05.041

[34] Y. Gan D. Zhao, B. Qin, X. Bi, Y. Liu, W. Ning, R. Yang, and Q. Jiang, "Numerical Simulation of High-Performance CsPbI$_3$/FAPbI$_3$ Heterojunction Perovskite Solar Cells," Energies, **15**(19), 7301 (2022). https://doi.org/10.3390/en15197301

[35] E. Danladi, M.Y. Onimisi, S. Garba, R.U. Ugbe, J.A. Owolabi, O.O. Ige, G.J. Ibeh, and A.O. Muhammed, "Simulation and optimization of lead-based perovskite solar cells with cuprous oxide as a P-type inorganic layer," Journal of the Nigerian Society of Physical Sciences, 72-81 (2019). https://doi.org/10.46481/jnsps.2019.13

[36] S.B. Zerarka Selssabil, M.Sc. thesis, "Study of electron transport effect on perovskite solar cells using simulation," University Mohamed Khider de Biskra, 2020.

[37] M.S. Rahman, S. Miah, M.S.W. Marma, and T. Sabrina, "Simulation based investigation of inverted planar perovskite solar cell with all metal oxide inorganic transport layers," in: *2019 International Conference on Electrical, Computer and Communication Engineering (ECCE)*, (IEEE, 2019).

[38] A.K. Das, R. Mandal, and D. Mandal, "Impact of HTM on lead-free perovskite solar cell with high efficiency," Optical and Quantum Electronics, **54**(7), 1-20 (2022). https://doi.org/10.21203/rs.3.rs-1366687/v1

[39] U. Mehmood, A. Al-Ahmed, F.A. Al-Sulaiman, M.I. Malik, F. Shehzad, and A. Ul Haq Khan, "Effect of temperature on the photovoltaic performance and stability of solid-state dye-sensitized solar cells: A review," Renewable and Sustainable Energy Reviews, **79**, 946-959 (2017). https://doi.org/10.1016/j.rser.2017.05.114

ДОСЛІДЖЕННЯ ВПЛИВУ ЕЛЕКТРОННИХ ТРАНСПОРТНИХ ШАРІВ, ДЕФЕКТУ ЩІЛЬНОСТІ ІНТЕРФЕЙСУ ТА РОБОЧОЇ ТЕМПЕРАТУРИ НА ПЕРОВСКІТНІ СОНЯЧНІ БАТАРЕЇ З ДОПОМОГОЮ ПРОГРАМНОГО ЗАБЕЗПЕЧЕННЯ SCAPS 1-D

Абубакар С. Юсуф[a,b], А.М. Рамалан[c], А.А. Абубакар[a], І.К. Мохаммед[a]

[a] Кафедра фізики, Федеральний технологічний університет, Р.М.В. 65, Мінна, Нігерія
[b] Кафедра фізики та астрономії, Оклендський технологічний університет, Нова Зеландія
[c] Кафедра фізики, Університет Абуджі, Р.М.В. 117, Абуджа, Нігерія

Перовскітні сонячні панелі привернули значну увагу дослідників сонячних панелей через їх потенціал для досягнення високої ефективності, в першу чергу, пов'язаних з їх винятковим транспортним шаром електронів (ETL). Матеріал ETL є однією з важливих компонентів перовскітних сонячних панелей в проведенні електронів для створення струму. Більше того, існує перспективний проспект для підвищення стабільності та зниження витрат на їх виготовлення шляхом заміни транспортного шару. У цьому конкретному дослідженні TiO$_2$ та SnO$_2$ використовувались як матеріали ETL в архітектурі перовскітної сонячної панелі для порівняльного аналізу між пристроями, що містять ріні структури: TiO$_2$/CH$_3$NH$_3$PbI$_3$/Spiro-OMeTAD та SnO$_2$/CH$_3$NH$_3$PbI$_3$/Spiro-OMeTAD. Для оцінки продуктивності кожного транспортного шару електронів (ETL) був використаний інструмент 1D SCAPS. Дослідження передбачало зміну товщини транспортних шарів електронів, щільності дефектів інтерфейсу та робочої температури, що дозволяє вичерпно оцінити пошук ключових параметрів таких як напруга на відкритому ланцюзі (VOC), щільність струму короткого замикання (JSC), коефіцієнт заповнення (FF) та загальна ефективність (PCE%). Примітно, що, використовуючи SnO$_2$ як ETL, досягнута ефективність становить 10,10 %. На відміну від цього, використання TiO$_2$ у якості ETL дає дещо більшу ефективність 12,84%. Ці знахідки підкреслюють нюанси впливу матеріалів транспортного шару на загальну продуктивність сонячних перовскітних батарей.

Ключові слова: *перовскіт; сонячна панель; SCAP-1D*